Structural and Multidisciplinary Optimization (2020) 61:2111–2123
https://doi.org/10.1007/s00158-019-02459-5

RESEARCH PAPER

Multi-objective optimization of crashworthiness of vehicle front longitudinal beam

Hangyan Wang[1] · Hui Xie[2]

Received: 29 August 2019 / Revised: 21 October 2019 / Accepted: 20 November 2019 / Published online: 14 December 2019

Abstract

Front longitudinal beam (FLB) is an important structure for the analysis of force transmission and energy absorption path in different crashing scenarios. In the present paper, the finite element (FE) model of a full-scale vehicle yun-100 Zotye is employed to explore the energy absorption of FLB, and aiming at its poor energy absorption problem, circular beam was used as the original topology optimization space of FLB. The advantages of both static and dynamic topology optimization methods are fully considered, and a variable density method is combined with a hybrid cellular automaton (HCA) method. The substructure dissipated energy and force for frontal crash in a full-scale vehicle are obtained at a speed of 13.8 m/s. The maximum stiffness in axial is obtained through the static topology optimization method and the maximum energy-absorbing structure of FLB which is satisfied with axial strength obtained through the dynamic topology optimization method. According to the results of topology optimization, a multi-cell thin-walled structure is interpreted as the novel FLB. A parametric study on geometric parameters is also performed to explore their effects on crashing characteristics of novel FLB, and it is found that they significantly influenced the crashworthiness of multi-cell thin-walled structure (especially the absorption of energy). Furthermore, in order to maximize the characteristics of novel FLB, a multi-objective optimization process is carried out using non-dominated sorting genetic algorithm (NSGA-II). The optimized FLB after multi-objective optimization is applied to Zotye of 100% vehicle frontal crash. The results showed that the peak value of acceleration decreased by 10.3% and the mass of the optimized FLB reduced to 0.59 kg. It indicated that the optimized FLB manifested excellent crashworthiness and better protective characteristics.

Keywords Crashworthiness · Front longitudinal beam (FLB) · Hybrid cellular automaton (HCA) · Parametric study · Non-dominated sorting genetic algorithm (NSGA-II)

1 Introduction

The crashworthiness of frontal collision of any vehicle examines the deformation mode and the energy absorption characteristics of front longitudinal beam (FLB) under various collision conditions (Kirkpatrick et al. 2001; Teng et al. 2008) and helps in reducing the degrees of damage of occupants by decelerating the vehicle. FLB is the main energy absorber in front crash accidents and absorbs almost 60% of total collision energy (Abramowicz 2003; Pashah et al. 2008). Therefore, the proper optimization of FLB structure can improve the crashworthiness of any vehicle by fulfilling the necessary safety requirements.

The crashworthiness of FLB is an indispensable research topic for vehicle crash safety. In the 1960s, Alexander (1960) studied the axial collision energy absorption characteristics of circular pipes. Huh et al. (2003) investigated the collision performance of FLB with and without considering the forming effect. Sun et al. (2017) studied the impact behavior of tubular-hydroformed axial crush tubes and revealed that the crashworthiness characteristics of FLB are influenced by many structural factors, such as cross-sectional configurations, manufacturing processes, effective length, wall thickness, and material properties.

Responsible Editor: Ren-Jye Yang

✉ Hangyan Wang
wanghangyan2017@163.com

[1] School of Mechanical and Automotive Engineering, Xiamen University of Technology, Xiamen 361024, Fujian, People's Republic of China

[2] State Key Laboratory of Advanced Design and Manufacturing for Vehicle Body, College of Mechanical and Vehicle Engineering, Hunan University, Changsha 410082, People's Republic of China

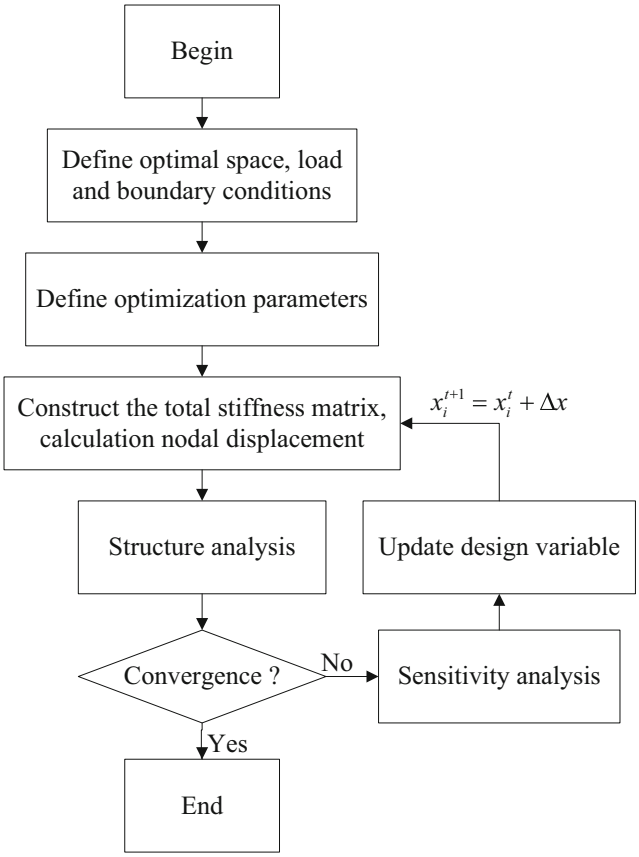

Fig. 1 Flowchart of static topology optimization

In the earlier days, engineers used to design any vehicle part based on their personal experiences and a significant amount of computer-aided analysis and optimization. Hence, the usage of manpower and material resources was high as well as the scope of optimization was limited. Therefore, it is necessary to propose a new method for designing the crashworthiness of FLB. Mayer et al. (1996) introduced the topological optimization method into the problem of structural crashworthiness and adopted the homogenization method to conduct the anti-collision optimization of body beam structure. Li et al. (2013) proposed an approach for reliability-based topology optimization of interval parameter structures under dynamic loads. Farahani et al. (2003) employed HEEDS software to analyze the topology optimization of a certain girder. Ortmann and Schumacher (2013) solved the topology optimization problem of dynamic loading by mathematical optimization algorithm and obtained the final optimization result of each design objective by solving the motion form of each key node.

In recent years, topology optimization is widely used in industrial design. However, traditional topology optimization methods usually consider static load effects and ignore dynamic load conditions. The hybrid cellular automaton (HCA) is an effective method for structural topology optimization and calculates strain energies by finite element method. NSGA-II, the improved version of non-dominated sorting genetic algorithm (NSGA), manifests excellent exploration performance (Deb et al. 2002; Marzbanrad and Ebrahimi 2011); hence, for multi-objective optimization of FLB, it can be used in combination with the results of topology optimization (Peng et al. 2016).

In the present study, a full-scale vehicle collision model was first established for China new car assessment program (C-NCAP) analysis, and the results revealed that the design of FLB was unreasonable. Therefore, the static topology optimization of FLB was performed by considering cylinder as the optimized object, and the dynamic topology optimization was carried out by taking stiffness and energy control as design objectives. Thus, the optimal material distribution was obtained and the novel FLB was obtained through engineering interpretation. Furthermore, a parametric study on energy absorption and crash characteristics was performed to compare different geometric parameters. In order to improve the crashworthiness of parameterized novel FLB by enhancing the specific energy absorption (SEA) and lowering the maximum crushing force, NSGA-II algorithm was employed. Finally, the optimized FLB was incorporated into the finite element model of a full-scale vehicle for simulation analysis and verification.

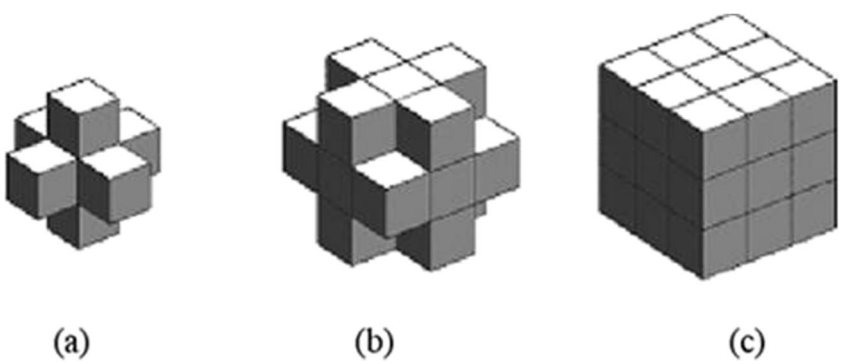

Fig. 2 Typical 3D CA neighborhoods: **a** von Neumann ($\hat{N} = 6$), **b** Radial ($\hat{N} = 18$), and **c** Moore ($\hat{N} = 26$)

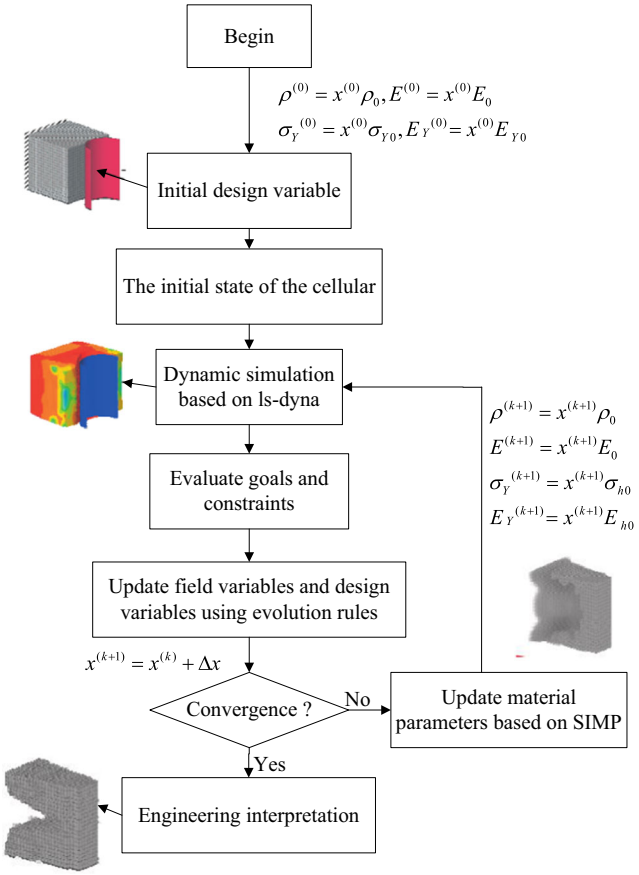

Fig. 3 Flowchart of the HCA method for crashworthy design optimization

2 Methodology

2.1 SIMP model based on variable density theory

In recent years, topology optimization has attracted immense research attention in both theoretical studies and practical applications (Wang et al. 2018a, b; Sigmund 2007). Currently, three common methods are generally adopted for continuous body topology optimization, i.e., alterable density method, homogenization method, and variable density method (Sigmund 1997), and among them, variable density method is commonly employed for structural optimization, especially for continuous structures. Therefore, the optimization problem

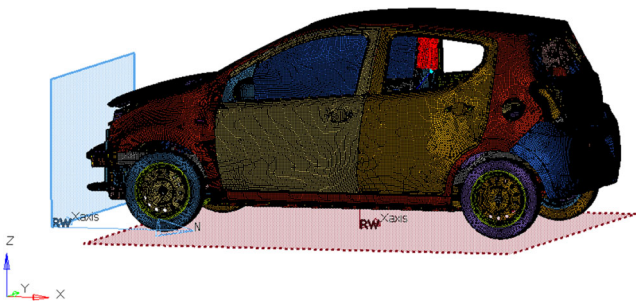

Fig. 4 Complete finite element model of Zotye

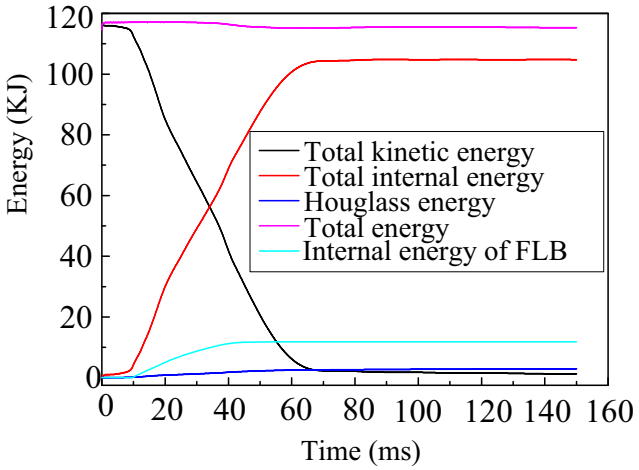

Fig. 5 Time history of energy

can be used to solve the optimal distribution scheme of materials in the structure. Solid isotropic material penalization (SIMP) is the most common interpolation model for variable density method, and it assumes that the density of material in the basic structure can vary. The nonlinear relationships between material parameters and material density established by SIMP can be formulated using the following Eq. (1):

$$\begin{aligned} \rho_i(x_i) &= x_i\rho_0 \\ E_i(x_i) &= x_i^p E_0 \\ K_i(x_i) &= x_i^p K_0 \\ \sigma(x_i) &= x_i^p \sigma_0 \\ 0 < x_i &< 1 \\ p &\geq 1 \end{aligned} \tag{1}$$

where x_i is the relative density of unit i, $p_i(x_i)$ is the material density of unit i, $E_i(x_i)E_i(x_i)$ is the material elastic modulus of unit i, $K_i(x_i)$ is the material stiffness of unit i,p_0 is the density of base material, E_0 is the elastic modulus of base material, and $K_0$is the stiffness of base material, and p is a penalization

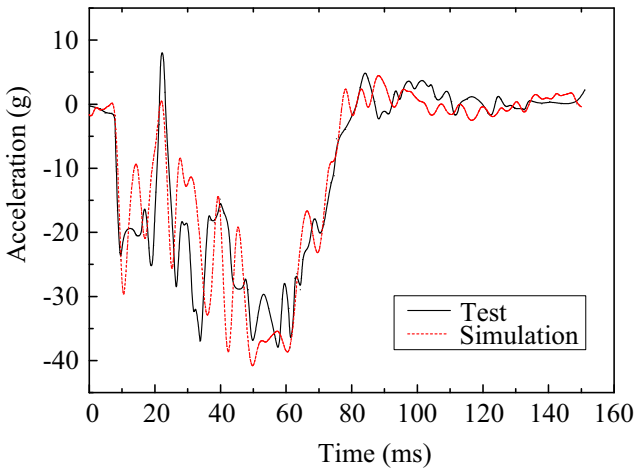

Fig. 6 Comparison between test and simulation for the acceleration of B pillar

Fig. 7 Comparison of global deformation between test and numerical simulation

parameter. The different values of p have a great influence on the calculation results of SIMP interpolation model.

2.2 Topology optimization based on the SIMP method

In structural stiffness optimization, the structure with high stiffness can be obtained by optimizing the minimum compliance, which can be expressed by the following Eq. (2):

$$C = F^T U = U^T K U \tag{2}$$

where C denotes compliance, $F$is the external load, $U$is the displacement of the structure, and $K$is the stiffness of the structure.

Considering the relative density of material as the design variable, the compliance of the structure as the optimization objective, and the mass fraction of target as the constraint condition, the optimal mathematical model is formulated as (3):

$$\begin{cases} \text{find } x = [x_1 x_2 \ldots x_n]^T \\ \min C(x) = U^T K U \\ s.t. F = KU \\ \sum_{i=1}^{n} (m_i/m_0) \le M^f \\ 0 < x_{\min} \le x_i \le x_{\max} \le 1 \end{cases} \tag{3}$$

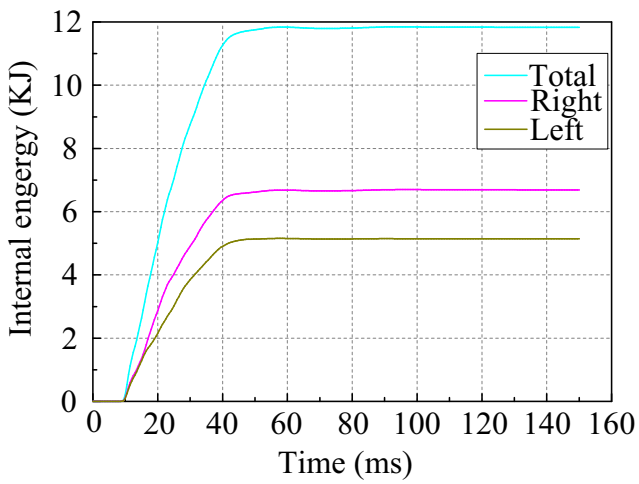

Fig. 8 Energy absorption of FLB

where m_i is the mass of unit i, m_0 is the initial total mass, and M^f is the mass fraction of target. In order to avoid the singularity of the total stiffness matrix, the design variable x_i is usually taken as 0.001.

In general, the SIMP interpolation model is solved by the OC method. In the process of optimizing the model by OC method, the related attributes of the structure are needed, and it can be obtained by sensitivity analysis.

1) Partial derivative of load $\frac{\partial F}{\partial x_i}$

Since the load is a constant independent of the design variable, take the partial derivative of it as (4):

$$\frac{\partial F}{\partial x_i} = 0 \tag{4}$$

2) Partial derivative of displacement $\frac{\partial U}{\partial x_i}$

According to the finite element equilibrium equation and the symmetry characteristic of the assembled stiffness matrix of the structure, the partial derivatives of the design variables are obtained on both sides, as follows (5):

$$\begin{aligned} \frac{\partial K}{\partial x_i} U + K \frac{\partial U}{\partial x_i} = 0 \\ \frac{\partial U^T}{\partial x_i} K + U^T \frac{\partial K}{\partial x_i} = 0 \end{aligned} \tag{5}$$

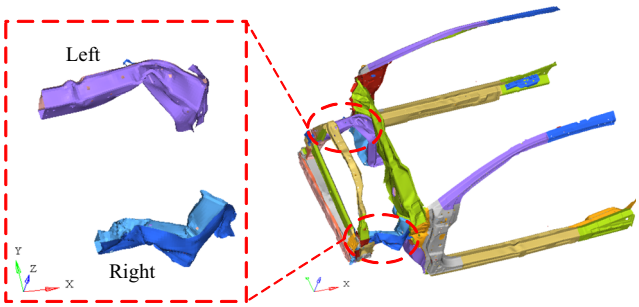

Fig. 9 Deformation of FLB

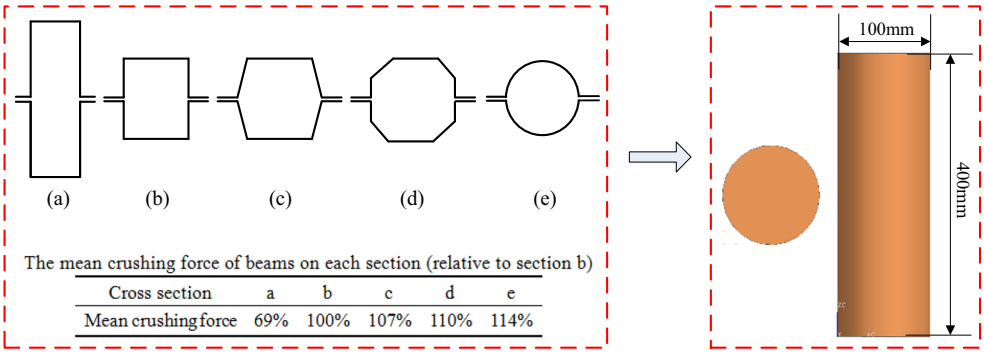

The mean crushing force of beams on each section (relative to section b)

Cross section	a	b	c	d	e
Mean crushing force	69%	100%	107%	110%	114%

Fig. 10 Initial optimization space for FLB

3) Partial derivatives of structural mass $\frac{\partial M}{\partial x_i}$

Since the structural the partial derivatives of the design variables are obtained on both sides, as follows, the formula is$M = \sum_1^n x_i m_i$, and the partial derivatives of the mass is obtained as follows (6):

$$\frac{\partial M}{\partial x_i} = \sum_1^n m_i \tag{6}$$

4) Partial derivative of the overall compliance$\frac{\partial C(x)}{\partial x_i}$

Since the objective function is $C(x) = U^T K U = \sum_1^n x_i^p u_i^T k_0 u_i$, the partial derivative can be obtained as (7):

$$C(x_i) = \frac{\partial C(x)}{\partial x_i} = \frac{\partial U^T}{\partial x_i} KU + U^T \frac{\partial K}{\partial x_i} U + U^T K \frac{\partial U}{\partial x_i} \tag{7}$$

In the current paper, in order to obtain the maximum stiffness of the structure, a static topological optimization method based on SIMP model was adopted. The basic flowchart of static topology optimization is depicted in Fig. 1.

2.3 Topology synthesis using the hybrid cellular automaton method

Cellular automata (CA) was first proposed by NEUMANN in the 1950s in order to simulate intercellular self-organization phenomena in biological systems (Neumann 1996). In the 1980s, WOLFRAM employed CA instead of partial differential equations to describe complex nonlinear systems (Wolfram 1983). Hybrid cellular automaton (HCA) algorithm combines the elements of CA with finite element analysis (FEA) (Tovar 2004), and this methodology is computationally efficient to solve topology optimization problems (Tovar et al. 2006). Figure 2 exhibits three typical examples of 3D CA neighborhoods.

In comparison to traditional CA, HCA adopts the local control law in order to make the effective field state ($\overline{U}_i(x_i)$) as close as possible to the target of strain energy density (U_i^*). Therefore, in HCA, strain energy density (SED), relative density (x_i), and uniform strain energy density are considered

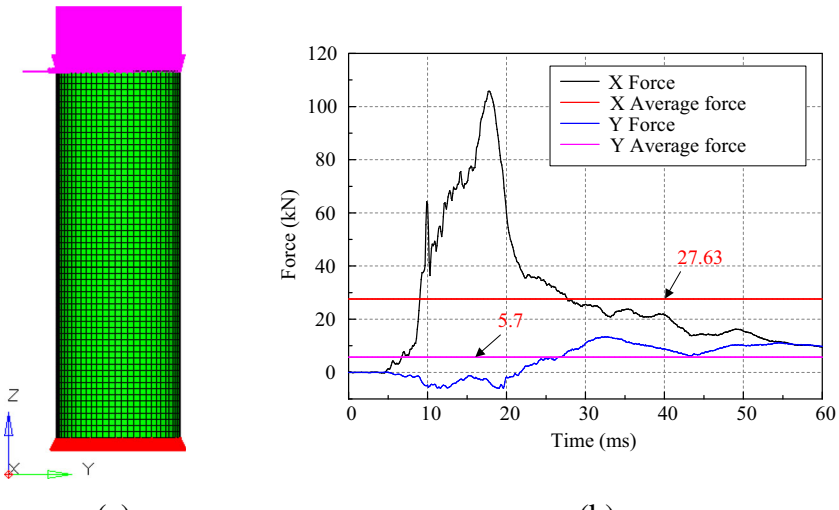

Fig. 11 Schematic representation of **a** quasi-static axial crushing and **b** crashing force

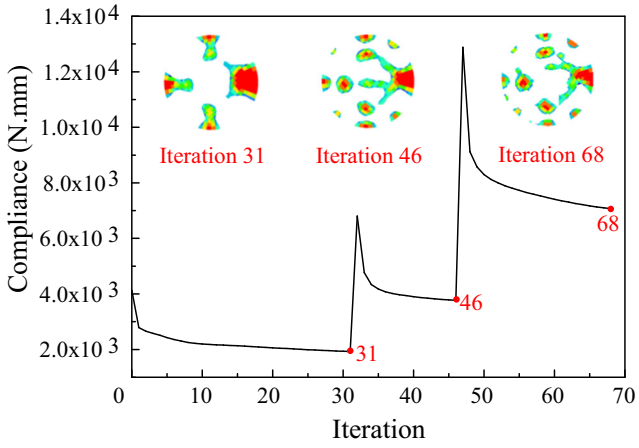

Fig. 12 Iterative process of static topology optimization

the field variable, the design variable, and the optimization objective, respectively, as follows (8):

$$\begin{cases} \text{find } x_i, (i = 1, 2, ..., n) \\ \min \sum_{i=1}^{N} \left| \overline{U}_i(x_i) - U_i^* \right| \\ s.t. \sum_{i=1}^{N} |\rho(x_i) v_1 / m_t| \le w_t \\ M\ddot{D}(t) + C\,D(t) = F(t) - R(D,t)\; 0 < x_{\min} \le x_i \le x_{\max} \le 1 \end{cases} \tag{8}$$

where N is the total number of cellular in the model; $\rho(x_i)$ is the density of the ith cellular; v_i is the volume of the ith cellular; m_t is the initial total mass; w_t is the mass fraction of target; $x_{\min}$ and $x_{\max}$ are, respectively, the upper and the lower boundaries of design variable constraint; M, C, and Ksignify mass, damping matrix, and stiffness matrix of the structure, respectively; $R$is the residual energy formed due to structural deformation; and D and F are the time-dependent structural displacement and force vector, respectively.

In addition, $\overline{U}_i(x_i)$ of a cellular reflects the average structural performance of itself and its neighborhood. It can be given by (9):

$$\overline{U}_i(x_i) = \frac{U_i(x_i) + \sum_{j=1}^{\hat{N}} U_j(x_j)}{\hat{N} + 1} \tag{9}$$

where $U_j(x_j)$ is the state of the ith neighbor and $\hat{N}$ is the total number of neighbors in the neighborhood of the ith cellular (Patel et al. 2009). In our study, von Neumann neighborhood with $\hat{N} = 6$ was selected for HCA optimization. The HCA method for crashworthy design optimization is illustrated in Fig. 3.

3 Optimization problem of FLB

3.1 Finite element collision analysis of the vehicle

The finite element (FE) frontal impact mode of a full-scale vehicle yun-100 Zotye (Fig. 4) is used in our research to explore the energy absorption capacity of FLB. It mainly consisted of shell element meshes, and some parts are replaced by body mesh or surface mesh. It contained 558 parts, 1012195 units, 990,824 nodes, and a total mass of 1179 kg. According to the requirements of China-New Car Assessment Program (C-NCAP), the speed of collision is 13.8 m/s (50 km/h). Several simulation observations revealed that the front collision energy absorption of FLB tended to be stable after 120 ms; hence, in order to improve the efficiency of calculation, the simulation calculation time is set to 120 ms.

3.1.1 Validation of FE model

The changes in energy curves are presented in Fig. 5 in order to demonstrate the feasibility of front impact model. In addition, as the B pillar acceleration can reflect the energy absorption capacity and the stiffness performance of a vehicle and also it is easy to measure, it is used as the output area of vehicle acceleration curve. The frontal collision of the electric vehicle is tested in the early stage, and the deformation and the

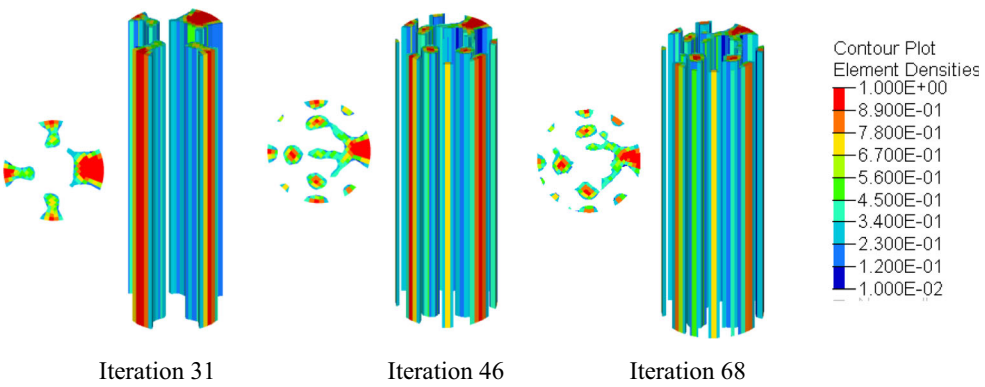

Fig. 13 Iterative process of topological optimization of front beam

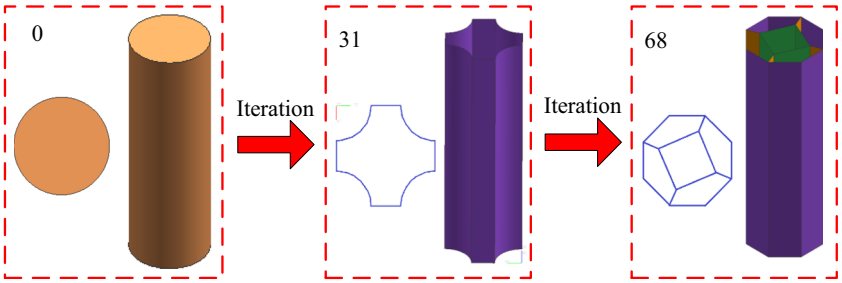

Fig. 14 Schematic representation of engineering interpretation of optimization results

acceleration curves are obtained. The comparison between acceleration curves obtained from the test and FE simulation is displayed in Fig. 6. The pulses are filtered by CFC 60 Hz according to the standard of Society of Automotive Engineers (SAE) J211. It is discernible that simulation results agreed well with the test. The values of peak acceleration of frontal impact are calculated as − 39 g and − 40 g in the test and FE simulation, respectively. Figure 7 compares the deformation of vehicle body after impact between test and FE simulation. It is evident that both the acceleration curve and the collision deformation pattern of FE simulation are consistent with the test results. Therefore, it can be inferred that our proposed numerical simulation of frontal collision is highly reliable and can replace the real collision scenario for relevant research.

3.1.2 Deformation and energy absorption of FLB

The energy absorption ability of FLB is not noticed within the first 10 ms (Fig. 8). During 10–17 ms, the energy absorption of FLB began to increase, and from 20 to 60 ms, the energy absorption ability increased rapidly. After 60 ms, the energy absorption tended to be stable and no longer increased. It is noticeable that the complete deformation of FLB occurred at 60 ms. The energy absorption are 5.1 kJ and 6.7 kJ for the left FLB and the right FLB, respectively. In addition, the total energy absorption of FLB is 11.8 kJ, which is only 11.3% of the total internal energy (104.7 kJ) (Fig. 5). The changes in axial and lateral impact cross-section forces of single FLB with time is presented in Fig. 11b. It is evident from Fig. 9 that the left FLB deformed in a global bending pattern and its energy absorption effect is not ideal, whereas the right FLB is less collapsed and its energy absorption capacity is not satisfactory. Therefore, in order to maximize the energy absorption capacity of FLB, the front of FLB should be collapsed layer by layer and the back of FLB should not be bent.

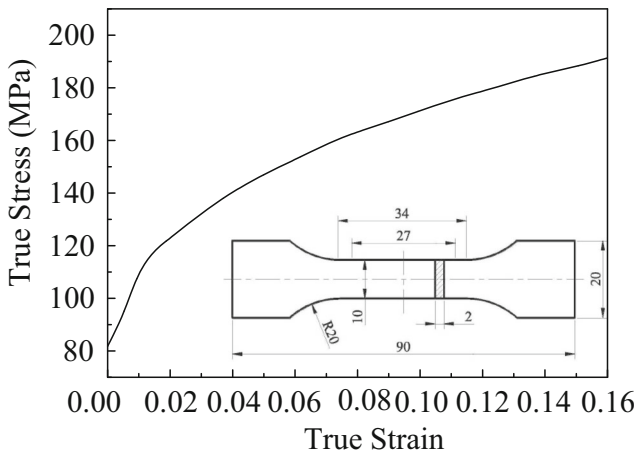

Fig. 15 Stress vs. plastic strain distribution for aluminum alloy AA6061-O

3.2 Topology optimization of FLB based on different performances

The cross-sectional shape of a thin straight beam significantly influences the collision energy absorption characteristics of a vehicle (Ren et al. 2018; Jiang et al. 2018). Sparke and Tomas (1994) conducted a comparative study on straight beams with different cross-sectional shapes and found that they had different collision resistance abilities; thus, when the cross-section of the beam is more angular and more rounded, its structural resistance is stronger (Fig. 10). Therefore, in order to obtain an optimal result from FLB, cylindrical solid is selected as the initial design optimization space for both static and dynamic topology optimization. Thus, a new type of FLB structure is obtained, and it meets the requirements of stiffness and energy absorption effect.

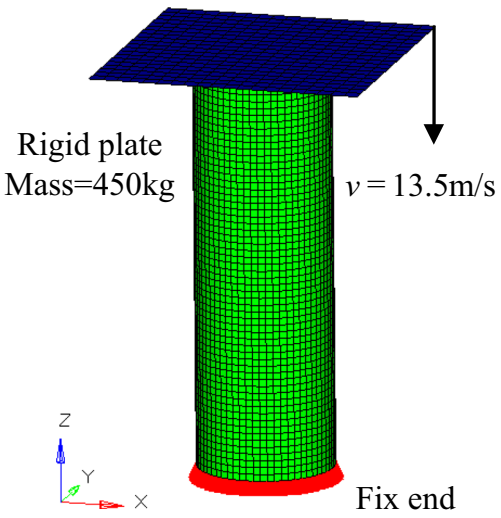

Fig. 16 Schematic representation of FE model

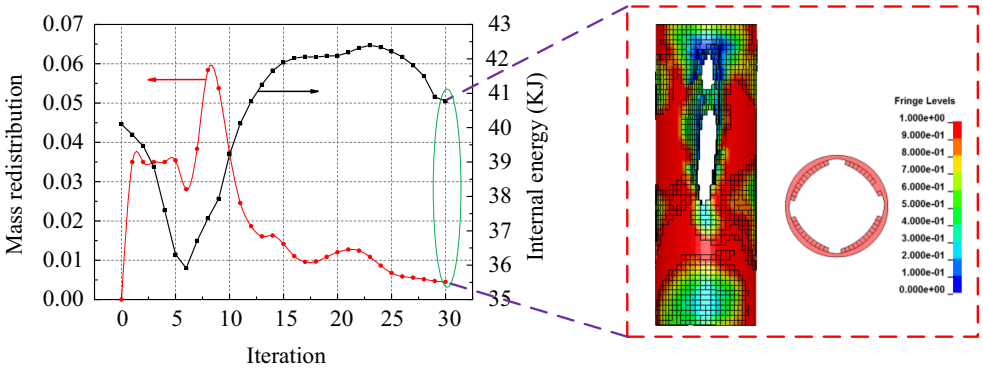

Fig. 17 HCA topology optimization results

From the simulation analysis of the vehicle, it is found that the FLB mainly relied on plastic deformation to absorb energy. During the collision process, it mainly bears the frontal impact force and the bending force caused by the deformation of bumper, and its energy absorption section is mainly concentrated in the first 400 mm. Therefore, a cylinder of 100-mm diameter and 400-mm length is selected for initial optimization in our research (Fig. 10).

The hexahedron is used to divide the grid into an average size of 5 mm; hence, the finite element model is developed to contain 29,280 shell elements and 31,720 nodes. With the increasing requirement of lightweight, aluminum alloy is extensively used in automobiles, and its energy absorption ratio is higher than that of steel. Therefore, in our paper, aluminum alloy of AA6061-O grade (density = 2580 kg/m^3, Poisson's ratio = 0.3, Young's modulus = 69 GPa, and initial yielding stress = 81 MPa) with an excellent forming performance is selected as the FLB material.

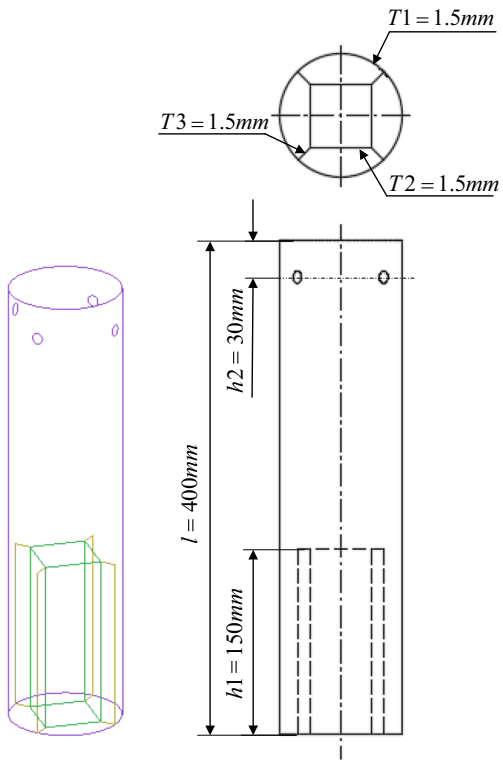

Fig. 18 Design of novel FLB based on engineering interpretation

3.2.1 Static topology optimization of FLB based on stiffness

Boundary conditions Vehicle collision is a dynamic nonlinear process, and the current topological optimization method is difficult to implement for this problem (Liu et al. 2017; Natke and Soong 1993). The simple and the effective way to solve this problem is to convert the impact load from FLB into static load. The peak of the collision force estimated the maximum load on vehicle body during the collision and it does not reflect the change in collision force during the entire collision. However, the optimization results obtained from peak impact force are usually over-designed. In comparison to peak collision force, the local average collision force ($\overline{P}$) emphasizes the change in collision force during the critical time period of the collision; hence, the optimization result is more reliable. In our paper, the local average collision force in the range of peak impact force is used as the equivalent static load, which is given by (10):

$$\overline{P} = \frac{\int_{S2}^{S1} F(s)ds}{S_2 - S_1} \tag{10}$$

where $F(s)$is the collision force with displacement in the peak area of collision force, and S_1 and S_2 are, respectively, the start and the end displacements within the peak range of collision force.

According to the frontal collision simulation, the mean value of axial load force and the lateral bending force during the

Table 1 Levels of geometric parameters

	Case 1	Case 0	Case 2
$t1$	1.5	2.0	2.5
$t2$	1.0	1.5	2.0
$t3$	1.0	1.5	2.0
$h1$	100	150	200
$h2$	20	30	40

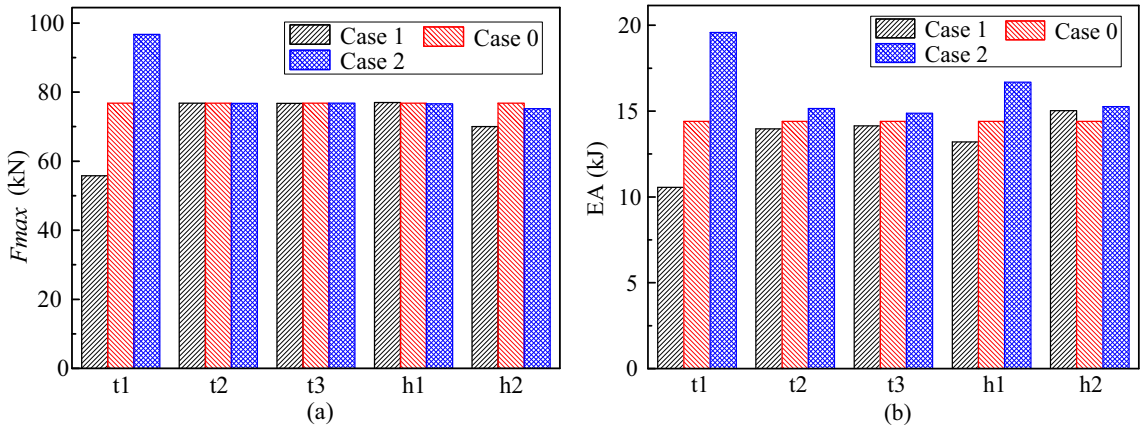

Fig. 19 Variations of **a** F_{max} and **b** EA for different design parameters

first 60 ms is set as the load boundary conditions (Fig. 11). Therefore, 27.63- and 5.7-kN loads are distributed, respectively, in the Z- and the Y-direction. In addition, 6 degrees of freedom is assigned to all nodes at the bottom of the cylinder.

In our analysis, the cell density of the cylinder is considered the design variable, the upper limit of constraint mass is 0.3, and the minimum compliance is assigned as the objective function. In order to obtain an equal-sectioned structure, the extrusion process constraints are added to the model along the vertical direction of the longitudinal beam. In addition, the minimum size of topological optimization is set to 15 mm in order to eliminate the gray level and also the phenomenon of checkerboard pattern.

Topology optimization results The iterative process of static topology optimization is displayed in Fig. 12. It can be noticed that convergence of the iteration is obtained after 68 steps. During the 31st, 46th, and 68th steps, the compliance of the cylinder fluctuated greatly due to a sharp change in the material. The topological optimization results for the 31st, the 46th, and the 68th iso-surfaces of 0.3 are presented in Fig. Error! Reference source not found.. After 60 iteration steps, the compliance of the cylinder gradually tended to be stable and axial stiffness reached its maximum value. It is also found that the compliance of the cylinder is minimum at the 31st iteration. Finally, the compliance tended to be stable after 68 iteration steps, and the mass constraint value is achieved.

As the middle unit of the cylinder is not the main load-bearing structure in our analysis, it is gradually deleted, and only the materials with severe force around the circumference are retained (Fig. 13). The topological optimization result of the 31st iteration could be considered a square tube with rounded corners around it. The topological optimization result of the 68th iteration can be interpreted as a multi-cell thin-walled structure, which has a regular octagonal shape on the outside and a quadrilateral cross-sectional shape on the inside. In addition, the four corners of the quadrilateral are connected with the four edges of the octagon for the sake of structural continuity (Fig. 14).

Table 2 Ranking of design variables according to their effects

Response	Design variables
F_{max}	$t1 > h2 > h1 > t2 > = t3$
EA	$t1 > h1 > h2 > t2 > t3$

3.2.2 HCA optimization of FLB based on crashworthiness

In Ls-dyna software, the finite element model for HCA topology optimization is established, and Mat-24 material is employed to simulate aluminum alloy. It is well known that high-strength steel is sensitive to strain rate and aluminum alloy has minimal strain effects; hence, the effect of strain rate on the aluminum alloy is not considered. The stress–strain curve of aluminum alloy AA6061-O is illustrated in Fig. 15.

Boundary conditions The collision process is simulated by assigning an initial velocity to the rigid plate. As the energy absorption of a single FLB in frontal collision accounted for about 30% of total collision energy and the total weight of the vehicle is about 1179 kg, 450 kg weight is assigned to the rigid plate (Fig. 16). The rigid plate is restrained by 5 degrees of freedom; thus, it could move only in the axial direction. The initial velocity and the grid size of the plate are 13.8 m/s and 10 mm, respectively. In addition, 6 degrees of freedom is

Table 3 Levels of design variables in initial iteration

Variables	Level		
	1	2	3
$t1$	1.5	2.0	2.5
$t2$	1.0	1.3	1.5
$t3$	1.0	1.3	1.5
$h1$	100	150	200
$h2$	20	30	40

Table 4 Responses of design variables in initial iteration

Run no.	$t1$	$t2$	$t3$	$h1$	$h2$	F_{max}/ kN	EA/ kJ	Mass/ kg
1	1	1	1	1	1	48.55	8.48	0.56
2	1	2	2	2	2	55.81	10.44	0.63
3	1	3	3	3	3	53.35	12.29	0.70
4	1	1	1	1	1	48.55	8.48	0.56
5	1	1	1	2	2	55.79	9.63	0.60
6	1	2	2	1	1	48.57	9.02	0.58
7	1	3	3	1	1	48.58	9.07	0.60
8	1	1	1	3	3	53.33	10.91	0.63
9	2	1	2	3	1	70.49	15.80	0.80
10	2	2	1	1	3	74.87	14.02	0.74
11	2	3	1	1	2	77.24	13.58	0.75
12	2	1	3	2	1	70.05	14.67	0.77
13	2	1	2	1	3	74.88	14.04	0.73
14	2	2	1	3	1	70.46	15.79	0.83
15	2	3	1	2	1	70.00	14.60	0.80
16	2	1	3	1	2	77.25	13.17	0.74
17	3	1	1	1	1	91.47	17.79	0.89
18	3	2	3	2	3	98.76	19.23	0.96
19	3	3	2	3	2	99.13	21.08	1.02
20	3	1	1	1	1	91.47	17.79	0.89
21	3	1	1	2	3	98.69	18.51	0.93
22	3	2	3	1	1	91.5	18.25	0.92
23	3	3	2	1	1	91.49	18.37	0.92
24	3	1	1	3	2	99.03	20.08	0.96
25	1	1	3	3	1	48.34	11.51	0.64
26	1	2	1	1	2	55.58	9.08	0.58
27	1	3	1	1	3	52.91	9.14	0.59
28	1	1	2	2	1	48.27	10.26	0.60
29	1	1	3	1	2	55.58	9.09	0.57
30	1	2	1	3	1	48.3	11.32	0.66
31	1	3	1	2	1	48.2	10.68	0.64
32	1	1	2	1	3	52.91	9.1	0.57

assigned to the bottom of the cylinder to make it completely fixed. Furthermore, in order to ensure good energy absorption characteristics and axial stiffness of FLB, the value of mass fraction is set to 0.3. This parameter describes the fraction of the mass of the part to be retained. The rest will be removed.

Topology optimization results The iterative process of quality allocation and the internal energy curve for dynamic topology optimization are displayed in Fig. 17. As the iteration progressed, the mass and the energy absorption capacity of the cylinder started to fluctuate due to the sharp changes in the material. The energy absorption gap between two iterations gradually became small, and finally, when the distribution of materials tended to be stable, the maximum value of internal energy is obtained. The iteration is completed after 30 steps, and a thin-walled circular structure is formed. In addition, some holes are formed on the surface of thin-walled circular structure; hence, local weakening is carried out in the positions where the holes are formed. Moreover, reinforcing bars are arranged at the positions where more materials are retained.

Table 5 Determination coefficient of each performance

	F_{max}/ kN	EA/ kJ	Mass/ kg
R^2	0.953	0.978	0.980

Table 6 Optimized design variables

Variable	$t1$/mm	$t2$/mm	$t3$/mm	$h1$/mm	$h2$/mm
Optimal	1.51	1.22	1.28	118.11	20.02
Rounding of optimal	1.50	1.20	1.30	118.00	20.00

3.2.3 Design of novel FLB

Although the results of static and HCA topological optimizations of the cylinder provided an important guidance for structural design, there is still a big gap with actual engineering; hence, the results are revised and re-designed based on actual situation and design experience. Based on the results, it is preliminarily considered that multi-cell thin-walled structure had the best cross-sectional form for FLB (Fig. 18). The height ($h1$) and the wall thickness ($t1 = t2 = t3$) of the square tube are 150 mm and 1.5 mm, respectively. In addition, four induction holes are opened at the upper end of the square tube in order to cause deformation. The distance from the center of the hole to the top of the sample ($h2$) is 30 mm, and the diameter of each hole is $\Phi = 10mm$.

3.3 Parametric analysis

In order to explore the crashworthiness characteristics of multi-cell thin-walled beam, a parametric study is performed to quantify the effects of$t1$,$t2$,$t3$,$h1$, and$h2$, and Table 1 summarizes the levels of these five geometric parameters. Case 0 indicates the initial size of novel FLB. Case 1 reduces the values of case 0, whereas case 2 increases the values of case 0.

Table 7 Error analysis of optimal design

Description	F_{max}/kN	EA/kJ	Mass/kg
Optimal (knee point)	44.57	9.02	0.58
FE model	48.95	9.32	0.59
Error	7.28%	3.22%	1.7%

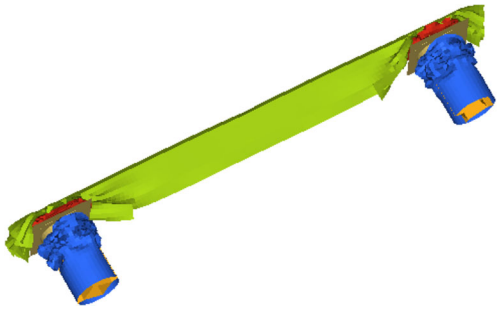

Fig. 20 The deformation model of the optimal FLB

Figure 19a and b display the histograms of F_{max} and EA, respectively. It is noticeable that all the parameters yielded different effects on the collision performance of FLB; specifically, $F_{max}$is strongly influenced by the thickness of $t1$, whereas EA is affected by all structural parameters.

For the maximum peak force, it increased linearly with $t1$. It is also found that the change of $h2$ had an influence on maximum peak force; however, $t2$, $t3$, and $h1$ yielded very little effect on maximum peak force. In addition, the energy absorption capacity of FLB is promoted with the increase in thickness, and the effect is most pronounced for $t1$. The energy absorption effect became worse with the increasing distances of the induction holes, and the energy absorption capacity of FLB is also influenced by the square tube height of secondary energy absorption. The relative importance of all design variables is presented in Table 2.

4 Design optimization of criss-cross structures

4.1 Optimization methodology

4.1.1 Definition of optimization problem

As an energy-absorbing structure, FLB is designed to improve its energy absorption capacity and also to reduce the maximum impact force; however, the improvement of energy absorption capacity always leads to an increase in vehicle mass (Wang et al. 2018a, b). It is also expected that FLB absorbs as much energy as possible under its unit mass. Hence, the maximization of energy absorption (EA) and the minimization of maximum peak crush force (F_{max}) are chosen as the objectives, while the mass (Mass) is chosen as the constraint for vehicle crashworthiness design. In Section 3.3, it is clearly presented that the effects of $t1$, $h1$, and $h2$ are more pronounced as compared to $t2$ and $t3$; thus, the ranges of $t2$ and $t3$ are reduced to diminish the search scope of optimization analysis. The optimization problem is formulated by the following mathematical expression (11):

$$\begin{cases} \min\{-EA(t1,t2,t3,h1,h2),\ F_{max}(t1,t2,t3,h1,h2) \\ \text{s.t.} \begin{cases} Mass(t1,t2,t3,h1,h2) \\ 1.5\ \text{mm} \le t1 \le 2.5\ \text{mm} \\ 1\ \text{mm} \le t2 \le 1.5\ \text{mm} \\ 1\ \text{mm} \le t3 \le 1.5\ \text{mm} \\ 100\ \text{mm} \le h1 \le 200\ \text{mm} \\ 20\ \text{mm} \le h2 \le 40\ \text{mm} \end{cases} \end{cases} \tag{11}$$

4.1.2 Surrogate model

The design variables are set in three levels, and the orthogonal array $L_{32}(5^3)$is used in the inner array (Table 3). Moreover, 32 sample points are inputted to the FE analysis software to extract the calculated results (Table 4).

Radial basic function (RBF) is more suitable for fitting nonlinear problems [29]; hence, the RBF modeling approach is chosen in our study to approximate the optimization objectives. The accuracy of RBF model is examined by the coefficient of determination R^2, which is given by (12):

$$R^2 = \frac{\sum_{i=1}^{n}\left(f_i - \overline{f}\right)^2}{\sum_{i=1}^{n}\left(\widetilde{f_i - \overline{f}}\sim\right)^2} \tag{12}$$

where $\widetilde{f_i}\sim$ is the function value calculated from the

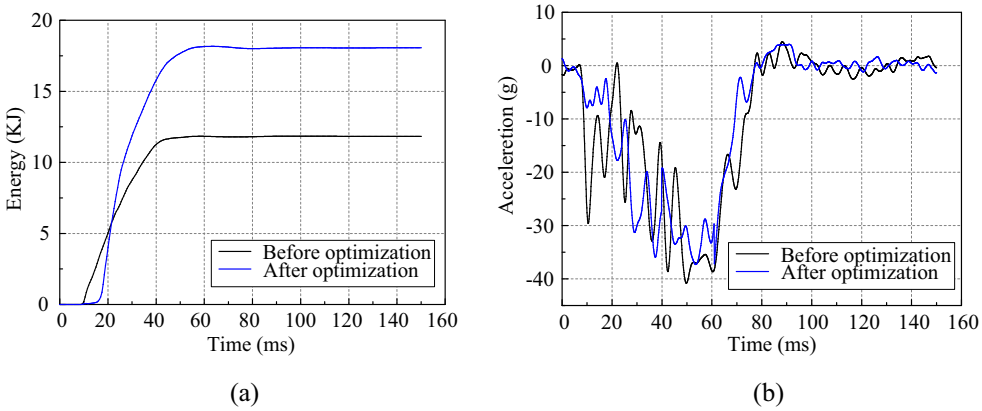

(a) (b)

Fig. 21 Time histories of performance before and after optimization: **a** energy and **b** acceleration

polynomial at the ith design point and $\overline{f}$ is the mean value of response sample point. The values of R^2 ranged from 0 to 1, and the accuracies of the surrogate model are higher when the values of $R^2$are closer to 1.

In our analysis, the determination coefficient of each performance of FLB is obtained (Table 5). It is found that the values of all coefficients are larger than 0.95; thus, these RBF surrogate models are applied to subsequent design optimization.

4.2 Optimization results

Deb et al. (2002) first proposed the NSGA-II algorithm by introducing fast non-dominant sorting method, elite retention strategy, and crowding comparison method in NSGA algorithm. In our analysis, NSGA-II algorithm is used to solve the multi-objective problem. The population and hereditary algebra are set to 200 and 100, respectively, and the total number of iteration is 20,000. Table 6 presents the details of optimized design variables, and the collision performance of FLB is depicted in Table 7. It can be found that the mass of optimized FLB is only 0.59 kg. It is also evident from Table 7 that there is a small difference between approximate optimal solutions and corresponding FEA solution; hence, it indicates the effectiveness of metamodel-based on FLB.

In order to further evaluate the reliabilities of optimization results, the optimized FLB is incorporated into the finite element model of a full-scale vehicle. The deformation model of the optimal FLB is extracted, as shown in Fig. 20. It is found that the front part is completely collapsed and could bear more energy absorption. Figure 21 displays the time histories of total internal energy and acceleration of novel FLB before and after optimization, respectively. It is noticeable that the energy absorption of optimized FLB is significantly improved, whereas the acceleration peak value of a full-scale vehicle decreased from 40.0 to 35.9 g, thus reducing the risks of injuries to its drivers and occupants. Therefore, it can be inferred that the proposed optimization method is promising for complex engineering design problems.

5 Conclusions

In the afore-discussed paper, static topology optimization and HCA are used to study the stiffness and the crashworthiness of FLB under frontal collision of a full-scale vehicle, and the multi-cellular thin-walled beam structure is obtained through the engineering interpretation of topological results. Moreover, for a better understanding of the relationship between crashworthiness criteria and geometric parameters ($t1$, $t2$, $t3$, $h1$, and $h2$), an parametric study is conducted. The results revealed that geometric parameters significantly affected the crashworthiness of multi-cellular thin-walled beam, and $t1$ experienced the most pronounced effect. Furthermore, the multi-objective optimization of FLB is carried out using NSGA-II algorithm in order to maximize and minimize the values of EA and F_{max}, respectively. Finally, the optimized FLB is applied to a full-scale vehicle model. It is found that the crashworthiness characteristics of the vehicle in terms of energy absorption and peak deceleration are enhanced significantly.

Funding information This work is supported by the strategic emerging industry of Hunan province and science technology research projects (2016GK4008).

Compliance with ethical standards

Conflict of interest The authors declare that they have no conflict of interest.

Replication of results All the necessary data to reproduce the results reported here are provided in Section 3.3 and Section 4.

References

Abramowicz W (2003) Thin-walled structures as impact energy absorbers. Thin-Walled Struct 41(2):91–107

Alexander JM (1960) An approximate analysis of the collapse of thin cylindrical shells under axial loading. Q J Mech Appl Math 13(1): 10–15

Deb K, Pratap A, Agarwal S, Meyarivan T (2002) A fast and elitist multiobjective genetic algorithm: NSGA-II. IEEE Trans Evol Comput 6(2):182–197

Farahani A, Averill RC, Sidhu R (2003) Design optimization of hydroformed crashworthy automotive body structures. In CAD-FEM Users' Meeting, 12–14

Huh H, Kim KP, Kim SH, Song JH, Kim HS, Hong SK (2003) Crashworthiness assessment of front side members in an autobody considering the fabrication histories. Int J Mech Sci 45(10): 1645–1660

Jiang H, Ren Y, Xiang J (2018) A numerical study on the energy-absorption of fibre metal laminate conical frusta under quasi-static compression loading. Thin-Walled Struct 124:278–290

Kirkpatrick SW, Schroeder M, Simons JW (2001) Evaluation of passenger rail vehicle crashworthiness. Int J Crashworthines 6(1):95–106

Li M, Tang W, Yuan M (2013) Structural dynamic topology optimization based on dynamic reliability using equivalent static loads. Struct Multidiscip Optim 49(1):121–129

Liu B, Huang X, Huang C, Sun G, Yan X, Li G (2017) Topological design of structures under dynamic periodic loads. Eng Struct 142: 128–136

Marzbanrad J, Ebrahimi MR (2011) Multi-objective optimization of aluminum hollow tubes for vehicle crash energy absorption using a genetic algorithm and neural networks. Thin-Walled Struct 49(12): 1605–1615

Mayer RR, Kikuchi N, Scott RA (1996) Application of topological optimization techniques to structural crashworthiness. Int J Numer Methods Eng 39(8):1383–1403

Natke HG, Soong TT (1993) Topological structural optimization under dynamic loads. Computer Aided Optimum Design of Structures III. Elsevier Science Publishers Ltd., 67–78

Neumann JV (1996) The theory of self-reproduction automata. University of Iuinois Press, Urbana, pp 64–87

Ortmann C, Schumacher A (2013) Graph and heuristic based topology optimization of crash loaded structures. Struct Multidiscip Optim 47(6):839–854

Pashah S, Massenzio M, Jacquelin E (2008) Prediction of structural response for low velocity impact. Int J Impact Eng 35(2):119–132

Patel NM, Kang BS, Renaud JE, Tovar A (2009) Crashworthiness design using topology optimization. J Mech Des 131(6):061013

Peng Y, Wang X, Xiong X, Xu P (2016) Crashing analysis and multi-objective optimisation of duplex energy-absorbing structure for subway vehicle. International Journal of Crashworthiness 21(4):338–352

Ren Y, Jiang H, Gao B, Xiang J (2018) A progressive intraply material deterioration and delamination based failure model for the crashworthiness of fabric composite corrugated beam: Parameter sensitivity analysis. Compos Part B 135:49–71

Sigmund O (1997) On the design of compliant mechanisms using topology optimization. Mech Struct Mach 25(4):493–524

Sigmund O (2007) Morphology-based black and white filters for topology optimization. Struct Multidiscip Optim 33(4–5):401–424

Sparke LJ, Tomas JA (1994) Crash pulse optimisation for minimum injury risk to car occupants. In SAFETY. TECHNICAL PAPERS FROM THE 25TH FISITA CONGRESS, BEIJING 4:945162

Sun G, Pang T, Fang J, Li G, Li Q (2017) Parameterization of criss-cross configurations for multiobjective crashworthiness optimization. Int J Mech Sci 124:145–157

Teng TL, Chang KC, Nguyen TH (2008) Crashworthiness evaluation of side-door beam of vehicle. Tech Mech 28(3–4):268–278

Tovar A (2004) Bone remodeling as a hybrid cellular automaton optimization process (Doctoral dissertation)

Tovar A, Patel NM, Niebur GL, Sen M, Renaud JE (2006) Topology optimization using a hybrid cellular automaton method with local control rules. J Mech Des 128(6):1205–1216

Wang H, Xie H, Liu Q, Shen Y, Wang P (2018a) Structural topology optimization of a stamping die made from high-strength steel sheet metal based on load mapping. Struct Multidiscip Optim 58(2):769-784

Wang H, Xie H, Cheng W, Liu Q, Shen Y (2018b) Multi-objective optimisation on crashworthiness of front longitudinal beam (FLB) coupled with sheet metal stamping process. Thin-Walled Struct 132:36–47

Wolfram S (1983) Statistical mechanics of cellular automata. Rev Mod Phys 55(3):601–644